International Journal of Mass Spectrometry 299 (2011) 35–46

Contents lists available at ScienceDirect

International Journal of Mass Spectrometry

journal homepage: www.elsevier.com/locate/ijms

Electrospray ionization mass spectrometry of a cerium(III) phosphomolybdate complex: Condensed and gas-phase cluster chemistry

Travis H. Bray, Roy Copping, David K. Shuh, John K. Gibson *

Chemical Sciences Division, The Glenn T. Seaborg Center, Lawrence Berkeley National Laboratory, Berkeley, CA 94720, USA

ARTICLE INFO

Article history:
Received 2 August 2010
Received in revised form 8 September 2010
Accepted 13 September 2010
Available online 17 September 2010

Keywords:
Electrospray ionization
Quadrupole ion trap
Phosphomolybdate
Polyoxometalate
Cerium
Collision induced dissociation

ABSTRACT

Electrospray ionization quadrupole ion trap mass spectrometry (ESI-QIT/MS) of the ammonium cerium(III) phosphomolybdate complex $(NH_4)_{11}[Ce(III)(PMo_{11}O_{39})_2]$ in aqueous media has revealed a concentration-dependent behavior. Under fixed instrumental parameters, the Ce-containing polyoxomolybdate complexes $H_2Ce(III)P_2Mo_{22}O_{75}{}^{3-}$ and $Ce(III)PMo_{11}O_{38}{}^{2-}$ are the primary species present at 11 mM (pH = 4.3); at 0.7 mM (pH = 3.6), $Ce(III)PMo_{10}O_{35}{}^{2-}$ is the predominant species, $Ce(III)PMo_{11}O_{38}{}^{2-}$ is quite diminished, and $H_2Ce(III)P_2Mo_{22}O_{75}{}^{3-}$ is absent. As a result of the complex isotopic fingerprints from multiple molybdenums, compositions of such ions are difficult to assign—successive collision induced dissociation (CID) of large ions produced smaller ions for which calculated and experimental isotopic patterns could be compared. The oxidation state of Ce and the number of counter cations on negative complexes was discerned from spectra of ions containing $^{1}H^{+}$ and $^{7}Li^{+}$. The overall result is an ESI method applicable to phosphomolybdate complexes containing redox sensitive *f*-block metal ions such as Ce(IV) and Pu(III/IV). Dissociation studies also gave insight into favored fragmentation pathways, and generated gas ions with empirical formulae similar to known condensed-phase ions. Deconvolution of concentration- and pH-dependent solution behavior via ESI/MS and ^{31}P NMR spectroscopy showed speciation dependent on solution concentration, not on pH.

© 2010 Elsevier B.V. All rights reserved.

1. Introduction

Polyoxometalates (POMs), metal-oxide clusters built from octahedral MO_6 units (typically M = Mo(VI) or W(VI)), have been extensively studied due to their wide array of applications [1]. The complex behavior of iso- and heteropolyoxometalates during transference from solution to gas has been determined from investigations via electrospray ionization mass spectrometry (ESI/MS) [2–11]. ESI, while a “soft” process in principle, has the potential to cause structural and chemical transformations of solution species during ion formation and transport. Concentration and pH changes during desolvation of aqueous droplets can induce structural changes in chemically sensitive molecules [12]. Ion-pairing and addition or loss of neutral species are possible consequences of ESI, and can increase the overall mass/charge ratio (m/z) [12]. An example of this effect is the protonation of surface oxygens and subsequent loss of neutral H_2O molecules from lacunary Keggin ions, e.g., $PMo_{11}O_{39}{}^{7-} + 4H^{+} \rightarrow PMo_{11}O_{37}{}^{3-} + 2H_2O$, which has been shown to be an effective method of reducing the charge of these POM ligands during the spray process [9]. Intriguing concentration-dependent behavior has also been reported by Bonchio et al., where Keggin ions reform through the formal uptake of $[WO]^{4+}$ by $PW_{11}O_{39}{}^{7-}$ in dilute solutions of $Li_7PW_{11}O_{39}$ [10]. The inherent electrochemistry of ESI can be used, for example, to employ the different redox properties of nickel and cobalt porphyrins for their independent detection from solution mixtures [13]. An additional ancillary complication of ESI is that fragmentation may occur during ion transport, prior to collection inside the ion trap. As a result of these potential ESI and gas-phase effects, it is common to observe numerous species resulting from a single solution precursor [12]. Until recently, collision induced dissociation (CID) results reported for POMs have focused on the preferred gas-phase degradation pathways of lacunary and plenary Keggin phosphotungstates. The recent seminal work of Ma et al. established a systematic approach to studying the CID fragmentation of these anions, as well as of the mixed metal Keggin derivatives $Co(II)PW_{11}O_{38}{}^{2-}$ and $Fe(III)PW_{11}O_{39}{}^{2-}$, the Dawson-Wells derivative $Co(II)P_2W_{17}O_{59}{}^{4-}$, and the Tourné sandwich anion derivative $Co(II)_4P_2W_{18}O_{65}{}^{4-}$ [11].

The potential presence of Keggin-based phosphomolybdate anions in nuclear waste spurred systematic solution and solid state investigations into their complexation of trivalent lanthanides [14,15]. These compounds form metal:ligand complexes, with the stoichiometries largely dependent on the metal-to-ligand ratios used during synthesis [16]. In the case of the **1:2** complex, $(NH_4)_{11}[Ce(PMo_{11}O_{39})_2]$, the structure has been determined and

---

* Corresponding author.
E-mail address: JKGibson@lbl.gov (J.K. Gibson).

1387-3806/$ – see front matter © 2010 Elsevier B.V. All rights reserved.
doi:10.1016/j.ijms.2010.09.015

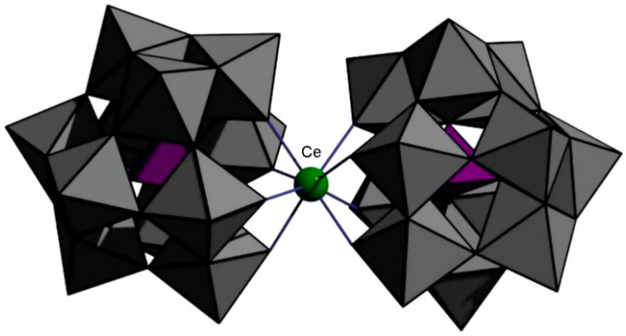

Fig. 1. Polyhedral representation of the solid state **1:2** Ce-phosphomolybdate complex $[Ce(PMo_{11}O_{39})_2]^{11-}$ [14].

reveals the Ce(III) metal ion resides in the vacancy of two lacunary phosphomolybdates (Fig. 1). This structure-type is found across the trivalent lanthanide series, as well as for the tetravalent metals Ce(IV) and Th(IV). Comparison of solution and solid-state IR and ^{31}P NMR provide evidence that these complexes are stable in solution and as solids. Although this system has been studied extensively in the condensed-phase [17,18], little has been reported regarding the gas-phase chemistry of POM-coordinated *f*-block metal complexes. However, ESI has been used as a characterization tool for lanthanide-phosphotungstate complexes [19]; the results reveal that these complexes can indeed be transferred to the gas phase, concurrent with evaporation of water to deplete surface POM oxygens [19]. We report the ESI behavior of the trivalent lanthanide lacunary phosphomolybdate complex $(NH_4)_{11}[Ce(III)(PMo_{11}O_{39})_2]$. Methods for identifying prominent cerium-phosphomolybdate species and determining the number of counter cations are described, which enables verification of the cerium oxidation state, Ce(III) or Ce(IV). A notable result is that these ligands stabilize cerium with respect to redox activity throughout the ionization and ion transport processes. An overarching goal of this work is to promote ESI/MS as a complementary investigative tool, along with solution and solid state spectroscopic and structural characterizations, for large inorganic complexes.

2. Experimental

2.1. Synthesis and preparation of complexes

Polyoxometalate salts were prepared as previously described: $(NH_4)_{11}[Ln(PMo_{11}O_{39})_2]$, Ln(III)POM where Ln = Ce, Pr, Eu or Tm [14,15,17]. In summary [15], $H_3PMo_{12}O_{40}$ was dissolved in H_2O with stirring and the pH adjusted by the addition of Li_2CO_3 to 4.3 to yield $[PMo_{11}O_{39}]^{7-}$ as the dominant phosphomolybdate species. $Ln(III)(NO_3)_3{\cdot}6H_2O$ was then added in a stoichiometric **2:1** PMo_{11}:Ln(III) ratio, resulting in a drop of ~1 pH unit. The pH was adjusted back to 4.3 by the addition of Li_2CO_3 and NH_4Cl. As in the previous work [15], ^{31}P NMR was used to confirm that the complex anion was present in solution. No free ligand was observed in solutions produced from precipitated Ln(III)POM salts. H_2O used in preparation of all solutions was microfiltered to 0.22 μm and purified to 18.5 MΩ using a Gradient A-10 Milli-Q distiller. All solutions were filtered with 0.2 μm nylon microfilters prior to ESI/MS or ^{31}P NMR measurements.

2.2. In situ dilution

Gaunt et al. reported crystalline structures corresponding to $(NH_4)_{11}[Ln(PMo_{11}O_{39})_2]{\cdot}16H_2O$ [14]; Copping et al. subsequently reported that bulk Ln(III)POM samples contain somewhat more water [15], as in $(NH_4)_{11}[Ce(PMo_{11}O_{39})_2]{\cdot}21H_2O$. In computing the solution concentrations, we employ the extent of hydration determined by Copping et al. [15] for materials prepared and handled under similar conditions as ours; although the reported absolute concentrations are considered uncertain by up to ~10%, the relative concentrations of the diluted solutions are accurate to within <5%. 11.2 mM Ce(III)POM solutions (pH = 4.4) were prepared by dissolving 60 mg Ce(III)POM in 1.3 mL H_2O. A syringe of the 11.2 mM solution was injected into the MS and spectra were acquired. The solution in the syringe was diluted by a factor of four, i.e. 20 μL 11.2 mM Ce(III)POM was diluted to 80 μL 2.8 mM by drawing 60 μL H_2O into the syringe; mixing was ensured by ejecting the solution into a small vial and redrawing it into the syringe. A 0.70 mM Ce(III)POM solution was similarly prepared by dilution of the 2.8 mM solution. In view of the concentration uncertainties, the concentrations of the three primary Ce(POM) solutions are referred to as 11 mM, 3 mM and 0.7 mM. Solutions of Ce(III)POM were also prepared at 3 mM (pH = 3.9) and 0.7 mM (pH = 3.6) by diluting an 11 mM stock solution. Additionally, 1.2–1.3 mM solutions of Ln(III)POM (Ln = Pr, Eu, and Tm) were prepared by dissolving 5.2 mg, 5.4 mg, and 5.0 mg of each salt, respectively in 1 mL H_2O.

2.3. pH dependence

The pH of an 11.2 mM solution of Ce(III)POM was adjusted with 0.1% HCl to values of 4.43, 3.96, 3.60, 3.20, and 2.84. Subsequent to each pH adjustment, an aliquot was removed for ESI/MS and a ^{31}P NMR spectrum was acquired from the remaining solution. Each pH adjustment equated to an addition of 1–2 drops of acid, thereby minimizing variations in the concentration of Ce(III)POM.

2.4. Concentration dependence

An 11.2 mM solution was diluted with water to concentrations of 5.6 mM, 1.1 mM, 0.56 mM, and 0.11 mM. After each dilution, the solution pH was adjusted back to 4.3 with 0.1% HCl or 1% NH_4OH. ESI/MS and ^{31}P NMR spectra were taken in a similar manner as with the pH dependence experiments.

2.5. Effect of metal:ligand ratio

ESI/MS and ^{31}P NMR spectra were taken before and after addition of one equivalent of Ce as $Ce(NO_3)_3{\cdot}6H_2O$ to an 11.3 mM solution of Ce(III)POM. The solution pH was adjusted back to 4.3 with 0.1% HCl and 1% NH_4OH.

2.6. ESI/MS

Experiments were performed with an Agilent 6340 Quadrupole Ion Trap (QIT) mass spectrometer with MS^n CID capabilities. In high resolution mode, the instrument has a detection range of 50–2200 m/z and resolution of ~0.25 m/z. Mass spectra were recorded in the negative ion detection mode. Spectra were taken with the following instrumental parameters: solution flow rate, 60 μl/min; nebulizer gas pressure, 15 psi; capillary voltage and current, 3500 V, 4.883 nA; end plate voltage offset and current, −500 V, 10 nA; dry gas flow rate, 5 l/min; dry gas temperature, 325 °C; capillary exit, −100 V; skimmer, −40 V; octopoles 1 and 2 DC, −12.00 V and −1.70 V; octopole RF amplitude, 108.9 Vpp; lenses 1 and 2, 5.0 V and 60.0 V; trap drive range, 99–149. Solutions were directly injected into the electrospray capillary using a syringe pump. Nitrogen gas was supplied from a vapor–liquid nitrogen dewar. CID experiments were performed using the He trapping gas; tickling voltages ranged between 0.30 V and 1.50 V, applied for 40 ms. The instrumental parameters were chosen to optimize the mass spectral intensity and resolution. No systematic study of the effects of drying gas temperature (or other instrumental parameters) was performed;

it is certainly feasible that speciation which is more representative of that in solution might be observed with lower drying gas temperatures, or other instrumental parameters.

The naturally occurring relative abundances of the elements studied are as follows: ^{92}Mo/61.5, ^{94}Mo/38.3, ^{95}Mo/66.0, ^{96}Mo/69.1, ^{97}Mo/39.6, ^{98}Mo/100.0, ^{100}Mo/39.9; ^{136}Ce/0.2, ^{138}Ce/0.3, ^{140}Ce/100.0, ^{142}Ce/12.3; ^{141}Pr/100.0; ^{151}Eu/91.6, ^{153}Eu/100.0; ^{169}Tm/100.0. The identities and charges of species were assigned by peak separation and experimental/computed isotopic pattern comparisons. The m/z values used to denote specific species correspond to the most abundant peak. As the isotopic patterns become complex with increasing number of molybdenum atoms, some isotopic identification comparisons were made following CID experiments, employing fragments with simpler isotopic patterns.

2.7. ^{31}P NMR

Spectra were taken on a Bruker Avance DPX$_{300}$. The number of scans was linear with solution concentration, from 10^3 scans for 11 mM solutions to 10^5 scans for 0.11 mM solutions.

3. Results and discussion

3.1. General considerations

In several instances, CID reactions produce either neutral ions or ions lying beyond the detection range of the mass spectrometer in high-resolution mode. The compositions of neutral species must be inferred. In all chemical equations, neutral species and ions which were not directly identified are shown in italics. Cerium phosphomolybdate fragments above the upper m/z limit of the spectrometer were inferred from the presence of the complementary low-m/z phosphomolybdate species. Species presumed to be present in solution prior to ESI are so indicated; all other species are in the gas phase. Protonation and evaporation of water from surface oxo-atoms can occur during ESI, such that the Mo/O ratios in ESI mass spectra are generally not indicative of the compositions of the oxygen-saturated polyoxometalate solution precursors. To assist in the confirmation of species identity, CID studies were conducted on prominent species to make comparisons between gas- and condensed-phase speciation.

3.2. Primary spectra

ESI/MS of Ce(III)POM solutions, acquired for the 11 mM, 3 mM, and 0.7 mM solutions, yielded distinct mass spectra after each successive dilution (Fig. 2). A key point is that the pH changes during the dilution, ranging from 4.3 at 11 mM, to 3.9 at 3 mM, to 3.6 at 0.7 mM. Dominant species produced from 11 mM solutions are the **1:2** and **1:1** complexes, $H_2Ce(III)P_2Mo_{22}O_{75}{}^{3-}$ and $Ce(III)PMo_{11}O_{38}{}^{2-}$. The **1:2** gas-phase complex, $H_2Ce(III)P_2Mo_{22}O_{75}{}^{3-}$, derived from the **1:2** solution complex, $[Ce(III)(PMo_{11}O_{39})_2]^{11-}$, is presumed to correspond to a cerium sandwiched between two phosphomolybdates, each containing 11 molybdenum atoms: where $(w+y)=75$ and $(x+z)=2$. As the distribution of oxygen and hydrogen atoms between the two phosphomolybdate ligands – i.e., the values of w, x, y and z – is not known, only the net formula of the gas-phase **1:2** complex is presented; the cerium sandwich complex structure is presumed. $H_2Ce(III)P_2Mo_{22}O_{75}{}^{3-}$ results from the protonation and dehydration of the solution precursor, $[Ce(III)(PMo_{11}O_{39})_2]^{11-}$.

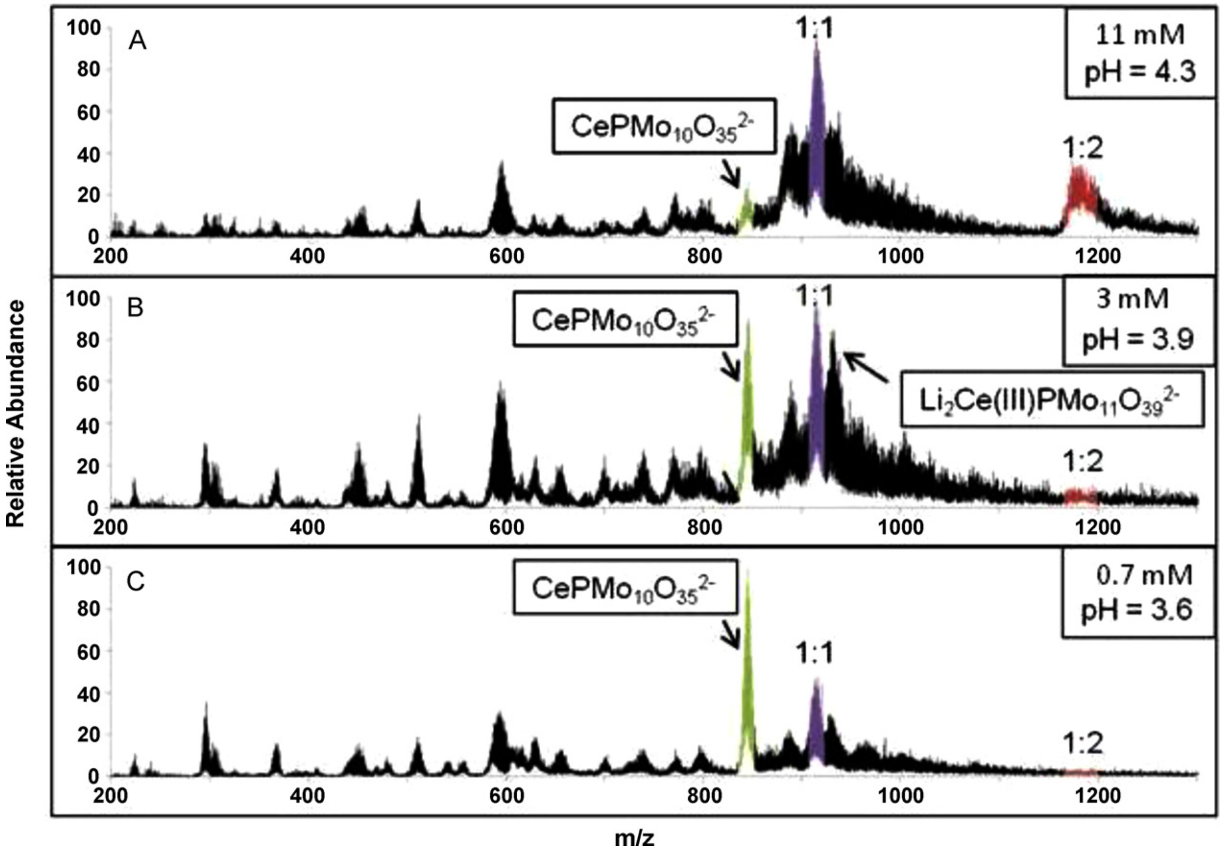

Fig. 2. Spectra of $(NH_4)_{11}Ce(III)(PMo_{11}O_{39})_{2(aq)}$ at (A) 11 mM, (B) 3 mM, and (C) 0.7 mM concentrations. The Ce-containing ions are identified: $Ce(III)PMo_{10}O_{35}{}^{2-}$, $Li_2Ce(III)PMo_{11}O_{39}{}^{2-}$, $Ce(III)PMo_{11}O_{38}{}^{2-}$ (**1:1**), and $H_2Ce(III)P_2Mo_{22}O_{75}{}^{3-}$ (**1:2**; only apparent in spectrum A).

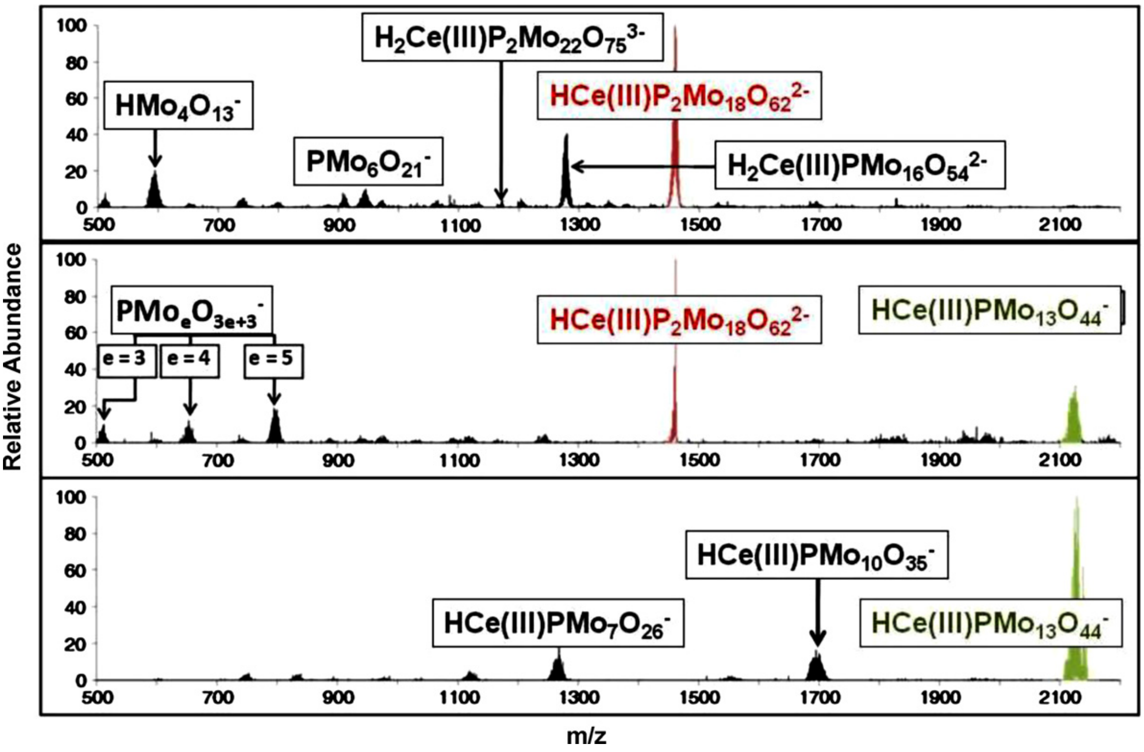

Fig. 3. Successive CID fragmentation spectra of (A) $H_2Ce(III)P_2Mo_{22}O_{75}{}^{3-}$, (B) $HCe(III)P_2Mo_{18}O_{62}{}^{2-}$, and (C) $HCe(III)P_2Mo_{13}O_{44}{}^{-}$.

Protonation of surface oxygens and ejection of three H_2O molecules from the solution species would account for the formation of $H_2Ce(III)P_2Mo_{22}O_{75}{}^{3-}$ during ESI, as represented by Eq. (1)

$$H_8[Ce(III)(PMo_{11}O_{39})_2]^{3-}_{(aq)} \xrightarrow{\text{ESI}} 3H_2O_{(g)} + H_2Ce(III)P_2Mo_{22}O^{3-}_{75(g)} \quad (1)$$

Similar effects during the spray process have been observed with both Ln-phosphotungstate complexes and bare ligands, such as $PMo_{11}O_{39}{}^{7-}$ [9,19]. Other major species in the parent spectrum (not labeled in Fig. 2A) include $HMo_aO_{3a+1}{}^{-}$ (a = 3–7), $Mo_bO_{3b+1}{}^{2-}$ (b = 2–5), $PMo_cO_{3c+3}{}^{-}$ (c = 3–5), and $Ce(III)PMo_dO_{3d+5}{}^{2-}$ (d = 4–10).

The assigned identity of the species at 1175 m/z, $H_2Ce(III)P_2Mo_{22}O_{75}{}^{3-}$, is supported by CID (Fig. 3). The primary fragmentation pathway of $H_2Ce(III)P_2Mo_{22}O_{75}{}^{3-}$ produces $HCe(III)P_2Mo_{18}O_{62}{}^{2-}$ by ejection of $HMo_4O_{13}{}^{-}$ (Eq. (2a); Fig. 3A). A second pathway also appears revealing degradation of $H_2Ce(III)P_2Mo_{22}O_{75}{}^{3-}$ to $H_2Ce(III)PMo_{16}O_{54}{}^{2-}$ by ejection of $PMo_6O_{21}{}^{-}$ (Eq. (2b)).

$$H_2Ce(III)P_2Mo_{22}O^{3-}_{75\ (g)} \xrightarrow{\text{CID}} HMo_4O^{-}_{13(g)} + HCe(III)P_2Mo_{18}O^{2-}_{62\ (g)} \quad (2a)$$

$$H_2Ce(III)P_2Mo_{22}O^{3-}_{75(g)} \xrightarrow{\text{CID}} PMo_6O^{-}_{21(g)} + H_2Ce(III)PMo_{16}O^{2-}_{54(g)} \quad (2b)$$

The identity of $HMo_4O_{13}{}^{-}$ is substantiated by direct comparison of experimental and calculated isotopic patterns. The identity of the CID product $PMo_6O_{21}{}^{-}$ is established by both its m/z position and CID behavior as compared to that of $PMo_6O_{21}{}^{-}$ in the primary spectra. Further isolation and fragmentation of $HCe(III)P_2Mo_{18}O_{62}{}^{2-}$ (Eq. (3a)–(3c)) yields the series of phosphomolybdate fragments, $PMo_eO_{3e+3}{}^{-}$ (e = 3–5), to form cerium-phosphomolybdates of the series $HCe(III)PMo_fO_{3f+5}{}^{-}$ (f = 13–15; Fig. 3B)

$$HCe(III)P_2Mo_{18}O^{2-}_{62(g)} \xrightarrow{\text{CID}} PMo_3O^{-}_{12(g)} + HCe(III)P_2Mo_{15}O^{-}_{50(g)} \quad (3a)$$

$$HCe(III)P_2Mo_{18}O^{2-}_{62(g)} \xrightarrow{\text{CID}} PMo_4O^{-}_{15(g)} + HCe(III)P_2Mo_{14}O^{-}_{47(g)} \quad (3b)$$

$$HCe(III)P_2Mo_{18}O^{2-}_{62(g)} \xrightarrow{\text{CID}} PMo_5O^{-}_{15(g)} + HCe(III)P_2Mo_{13}O^{-}_{44(g)} \quad (3c)$$

Major CID products of $HCe(III)P_2Mo_{13}O_{44}{}^{-}$ form through loss of either Mo_3O_9 or Mo_6O_{18}, as indicated in Eqs. (4a and 4b) (Fig. 3C)

$$HCe(III)PMo_{13}O^{-}_{44(g)} \xrightarrow{\text{CID}} Mo_3O_{9(g)} + HCe(III)PMo_{10}O^{-}_{35(g)} \quad (4a)$$

$$HCe(III)PMo_{13}O^{-}_{44(g)} \xrightarrow{\text{CID}} Mo_6O_{18(g)} + HCe(III)PMo_7O^{-}_{26(g)} \quad (4b)$$

Upon dilution to 3 mM (pH = 3.9), no detectable solution precursor, $H_2Ce(III)P_2Mo_{22}O_{75}{}^{3-}$, remains intact (Fig. 2B). Instead, the spectrum evolves with decreasing concentration such that the dominant species are $Ce(III)PMo_{10}O_{35}{}^{2-}$, $Ce(III)PMo_{11}O_{38}{}^{2-}$, and $Li_2Ce(III)PMo_{11}O_{39}{}^{2-}$; the origin of this last species, which contains Li, is discussed below. The spectrum continues to change at lower concentration (0.7 mM), with $Ce(III)PMo_{10}O_{35}{}^{2-}$ becoming the most prominent species (Fig. 2C).

3.3. *Lithiated species*

A pronounced 'tail' is observed at higher m/z in close proximity to the **1:2** $H_2CeP_2Mo_{22}O_{75}{}^{3-}$ complex (Fig. 2A). To determine the nature of this tail, CID studies were performed with the excitation voltage centered at 1170, 1180, and 1190 m/z, each after isolation with a width of 10 m/z (Fig. 4). As discussed above, the results at 1170 m/z indicates a species identified as $H_2Ce(III)P_2Mo_{22}O_{75}{}^{3-}$. Results at 1180 m/z and 1190 m/z indicate the presence of $H_gLi_{2-g}Ce(III)P_2Mo_{22}O_{75}{}^{3-}$ and $H_gLi_{4-g}Ce(III)P_2Mo_{22}O_{76}{}^{3-}$ where g = 0 or 1 (Fig. 4C and D); $Li_2Ce(III)PMo_{11}O_{39}{}^{2-}$ (933 m/z) is also present as a peak envelope centered around m/z 15 above $Ce(III)PMo_{11}O_{38}{}^{2-}$ (Fig. 2B). The identity of these partially lithiated species is supported again by CID. Both $H_gLi_{2-g}Ce(III)P_2Mo_{22}O_{75}{}^{3-}$ and $H_gLi_{4-g}Ce(III)P_2Mo_{22}O_{76}{}^{3-}$ (g = 0 or 1) fragment in a similar manner as $H_2Ce(III)P_2Mo_{22}O_{75}{}^{3-}$, through production of partially lithiated tetramolybdate, $[H/Li]Mo_4O_{13}{}^{-}$ and either $LiCe(III)P_2Mo_{18}O_{62}{}^{2-}$ (1465 m/z) or $Li_3Ce(III)P_2Mo_{18}O_{63}{}^{2-}$ (1480

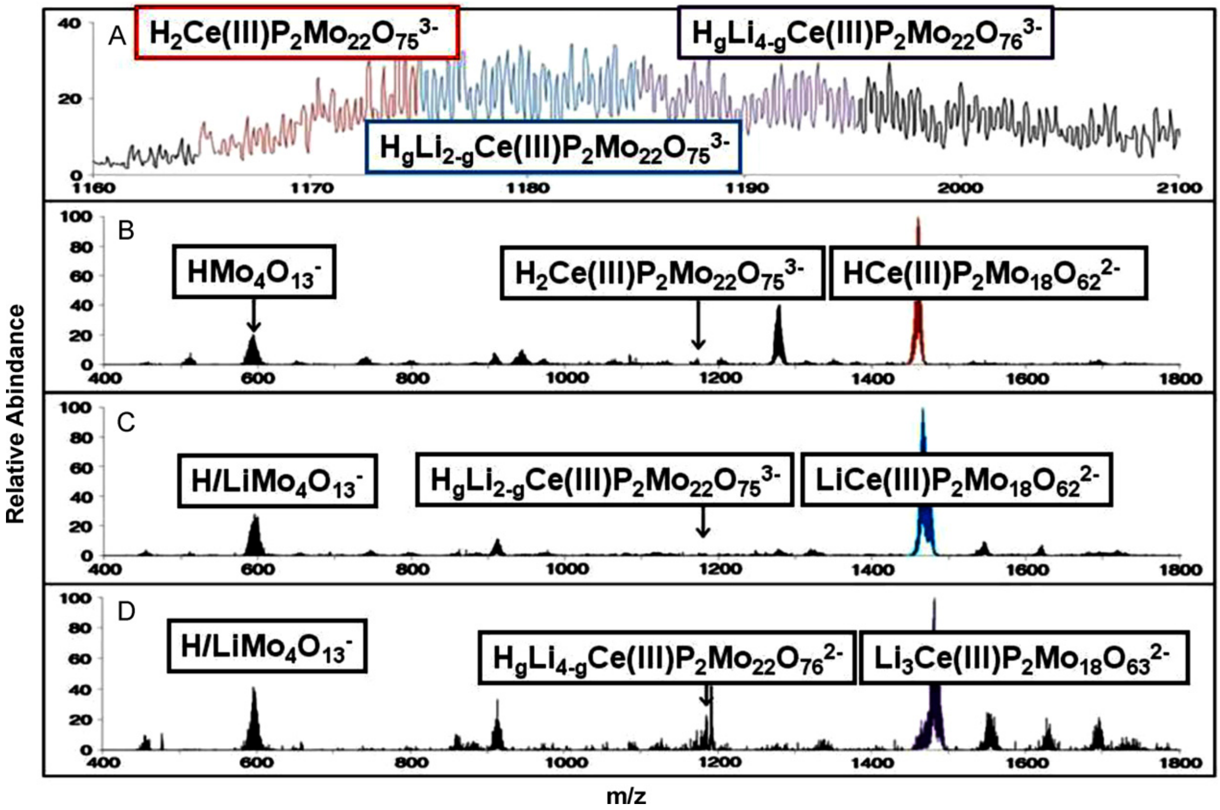

Fig. 4. (A) Spectra of Ce(III)POM highlighting $H_2Ce(III)P_2Mo_{22}O_{75}^{3-}$ (red), $H_gLi_{2-g}Ce(III)P_2Mo_{22}O_{75}^{3-}$ (blue), and $H_gLi_{2-g}Ce(III)P_2Mo_{22}O_{75}^{3-}$ (purple); $g = 0$, 1. CID of (B) $H_2Ce(III)P_2Mo_{22}O_{75}^{3-}$, (C) $H_gLi_{2-g}Ce(III)P_2Mo_{22}O_{75}^{3-}$, and (D) $H_gLi_{4-g}Ce(III)P_2Mo_{22}O_{76}^{3-}$, performed by isolating and fragmenting with mass range of 10 centered around 1170 *m*/*z*, 1180 *m*/*z*, and 1190 *m*/*z*, respectively ($g = 0$, 1). (For interpretation of the references to colour in this figure legend, the reader is referred to the web version of the article.)

m/*z*), respectively (Fig. 4C and D). Successive degradation of $H_gLi_{2-g}Ce(III)P_2Mo_{22}O_{75}^{3-}$ eventually forms $LiCe(III)PMo_7O_{26}^-$, in direct analogy to $HCe(III)PMo_7O_{26}^-$ from $H_2Ce(III)P_2Mo_{22}O_{75}^{3-}$. Apparently, Li^+ ions used to adjust the pH during the synthesis co-precipitate with H^+ and are carried over into the Ce(III)POM solutions. This allows for ion-pairing competition during desolvation. The result is the presence of lithiated species which, fortuitously, assist in determining the quantity and identity of cations present on the large **1:2** complexes in the gas phase.

The exact composition of $H_2Ce(III)P_2Mo_{22}O_{75}^{3-}$ is difficult to definitively establish. While successive CID events do support the assignment, instrumental limitations prevent direct comparison of experimental and calculated isotopic patterns of observed ions produced after several iterations of isolation and fragmentation, i.e. $>MS^4$. The molybdenum count in the ion $HCe(III)PMo_7O_{26}^-$ is supported by its *m*/*z* position at twice that of $Ce(III)PMo_7O_{26}^{2-}$, an ion observed in the primary spectra, as confirmed by CID (Fig. 5) [20]. Identification of a proton on a large multiply charged ion, especially those containing isotopically-rich elements such as Mo, is challenging given the resolution of the QIT/MS. The presence of the redox active Ce metal ion introduces additional complicating effects as it would be difficult to differentiate such ions as $HCe(IV)P_2Mo_{22}O_{75}^{3-}$ from $H_2Ce(III)P_2Mo_{22}O_{75}^{3-}$. However, successive degradation of $H_gLi_{2-g}Ce(III)P_2Mo_{22}O_{75}^{3-}$ to eventually form $HCe(III)PMo_7O_{26}^-$ yields an ion that can be directly compared to $LiCe(III)PMo_7O_{26}^-$. In particular, the two ions $HCe(III)PMo_7O_{26}^-$ and $LiCe(III)PMo_7O_{26}^-$, are separated by ~6 *m*/*z* (Fig. 6), supporting the proposition of substitution of H^+ by Li^+ and, therefore, the identity of $LiCe(III)PMo_7O_{26}^-$. These results also aid in assigning the proton count on $H_2Ce(III)P_2Mo_{22}O_{75}^{3-}$, $HCe(III)P_2Mo_{18}O_{62}^{2-}$, and $HCe(III)PMo_{13}O_{44}^-$, thereby indicating the trivalent oxidation state of cerium throughout. Although Ce(III) would not necessarily expected to be oxidized to Ce(IV) under the conditions of these experiments, confirming that cerium remains in the Ce(III) oxidation state from solution throughout the electrospray and CID processes is a useful methodology for oxidation state determination of redox active metal-complexes with f-block elements such as Ce(IV) and Pu(III/IV).

3.4. Thermodynamics of H_2O and Li_2O elimination

An interesting result is the successful transference of $[HLi_3/Li_4]Ce(III)P_2Mo_{22}O_{76}^{3-}$ and $Li_2Ce(III)PMo_{11}O_{39}^{2-}$ ions into the gas phase. Given the absence of the corresponding protonated

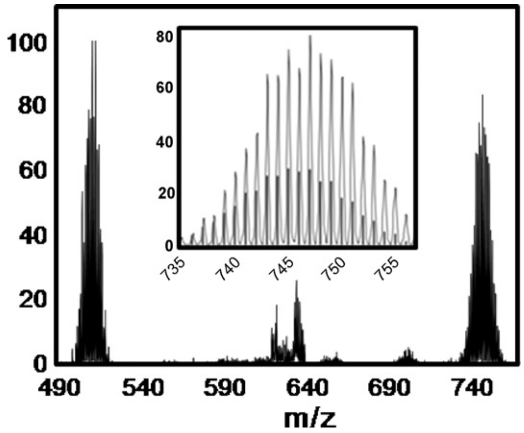

Fig. 5. CID spectra of $Ce(III)PMo_7O_{26}^{2-}$ yielding $PMo_3O_{12}^-$ (510 *m*/*z*) and $Ce(III)Mo_4O_{14}^-$ (747 *m*/*z*). Inset shows consistency between experimental (peaks) and calculated (bars) isotopic patterns of $Ce(III)Mo_4O_{14}^-$.

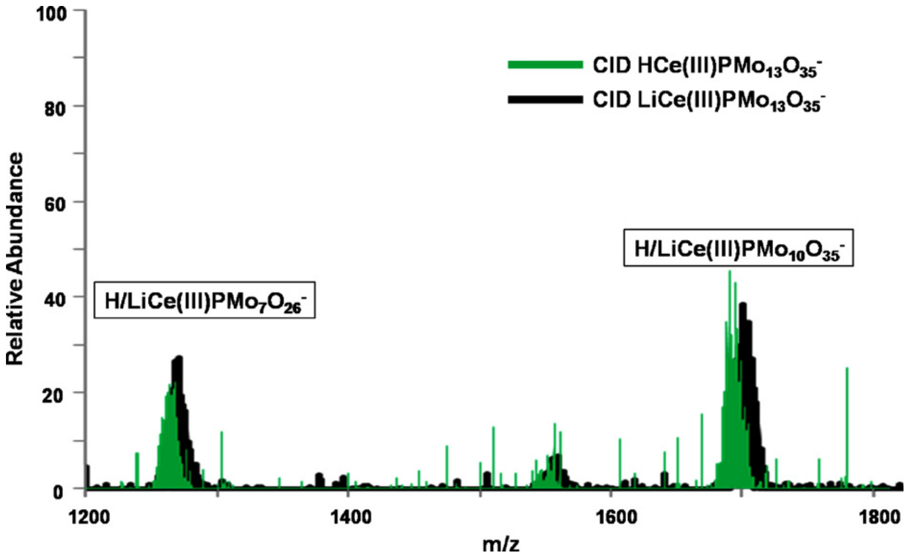

Fig. 6. CID products of $HCe(III)PMo_{13}O_{35}^{-}$ and $LiCe(III)PMo_{13}O_{35}^{-}$. A shift of 6 *m*/*z* is observed, consistent with the difference due to $^{7}Li^{+}$ substitution for $^{1}H^{+}$.

species, $H_4Ce(III)P_2Mo_{22}O_{76}{}^{3-}$ and $H_2Ce(III)PMo_{11}O_{39}{}^{2-}$, this suggests that multiply lithiated species are more stable with respect to Li_2O formation and loss as compared to protonated species and H_2O-loss. Simplistically, the comparative thermodynamics for H_2O- and Li_2O-elimination might be evaluated from the gas-phase reactions given by Eqs. (5a) and (5b).

$$H_4CeP_2Mo_{22}O_{76}{}^{3-} \rightarrow H_2Ce(III)P_2Mo_{22}O_{75}{}^{3-} + H_2O \qquad (5a)$$

$$Li_4CeP_2Mo_{22}O_{76}{}^{3-} \rightarrow Li_2Ce(III)P_2Mo_{22}O_{75}{}^{3-} + Li_2O \qquad (5b)$$

As the coordination energy of the H^+ and Li^+ counter ions to the $CeP_2Mo_{22}O_{76}{}^{7-}$ anions should be roughly comparable, the energy difference between Eqs. (5a) and (5b) could be approximated by the enthalpies for Eqs. (6a) and (6b), the first of which is more exothermic.

$$2H + O \rightarrow H_2O \quad \Delta H[6a] = -927\,\mathrm{kJ\,mol^{-1}} \qquad (6a)$$

$$2Li + O \rightarrow Li_2O \quad \Delta H[6b] = -734\,\mathrm{kJ\,mol^{-1}} \qquad (6b)$$

However, a more realistic assessment of H_2O and Li_2O elimination should consider the reactions and associated thermodynamics of the charged counter ions, H^+ and Li^+, to produce H_2O and Li_2O, as shown in Eqs. (7a) and (7b), where IE is the ionization energy and EA the electron affinity.

$$2H^+ + O^{2-} \rightarrow H_2O \quad \Delta H[7a] = \Delta H[6a] - 2\{\mathrm{IE}[H^+]\} - EA[O] - EA[O^-] = -3551\,\mathrm{kJ\,mol^{-1}} - \mathrm{EA}[O] - \mathrm{EA}[O^-] \qquad (7a)$$

$$2Li^+ + O^{2-} \rightarrow Li_2O \quad \Delta H[7b] = \Delta H[6b] - 2\{\mathrm{IE}[Li^+]\} - EA[O] - EA[O^-] = -1774\,\mathrm{kJ\,mol^{-1}} - \mathrm{EA}[O] - \mathrm{EA}[O^-] \qquad (7b)$$

Eq. (7a) is 1777 kJ mol^{-1} more exothermic than Eq. (7b), primarily due to the much higher IE[H] = 13.60 eV (1312 kJ mol^{-1}) compared to IE[Li] = 5.39 eV (520 kJ mol^{-1}). The conclusion of this elementary energetic analysis is that H_2O elimination from protonated oxides is thermodynamically much more favorable than Li_2O elimination from lithiated oxides, in accord with the experimental observations. The propensity to retain lithiated species in preference to protonated species, even with minor amounts of Li^+ ions available, can be attributed to the much higher ionization energy of hydrogen to produce H^+ counterions as compared with lithium to produce Li^+ counterions. It is anticipated that this should also be observed with heavier alkali metal ions, which could provide a new opportunity for greater mass separation than between ^{1}H and ^{7}Li.

3.5. *Solution versus gas-phase speciation by ESI and ^{31}P NMR*

3.5.1. *Varying M:L ratio*

Analysis of an 11 mM solution by ^{31}P NMR indicates the presence of two phosphorous complexes with chemical shifts of −5.8 ppm and −6.9 ppm (Fig. 7). A chemical shift of −5.6 ppm has been previously reported for the **1:2** solution complex, $[Ce(III)(PMo_{11}O_{39})_2]^{11-}$ [15]. The singlet at −5.8 ppm closely matches this value; the singlet at −6.9 ppm is then presumed to correspond to the **1:1** complex, $H_xCe(III)P_2Mo_{11}O_{39}{}^{(4-x)-}$; pH-dependent protonation of the **1:1** complex—i.e., the value of *x* – was indicated by the pH studies discussed in the next section. The above

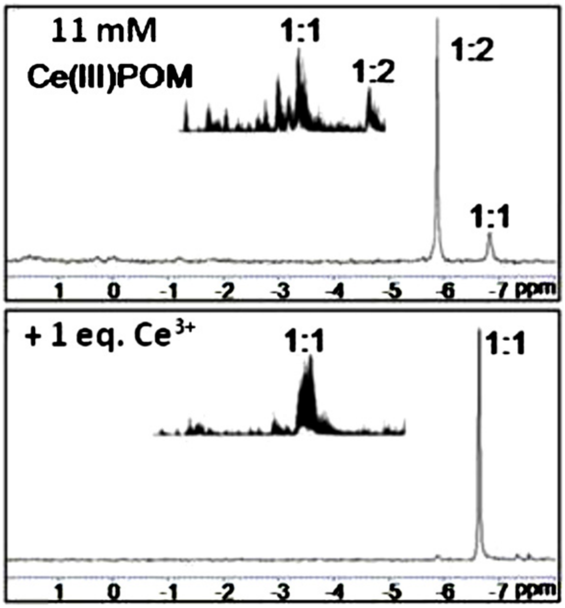

Fig. 7. ^{31}P NMR spectra of a 10 mM Ce(III)POM solution (top); and a 10 mM Ce(III)POM solution to which one equivalent of Ce^{3+}, as $Ce(NO_3)_3{\cdot}6H_2O$, was added (bottom). Inset shows ESI/MS spectra under the same conditions. Peak labels indicate the $Ce(III)PMo_{11}O_{38}{}^{2-}$ (**1:1**) and $H_2Ce(III)P_2Mo_{22}O_{75}{}^{3-}$ (**1:2**) complex ions; the solution compositions of the **1:1** and **1:2** ions are not the same as in the gas-phase.

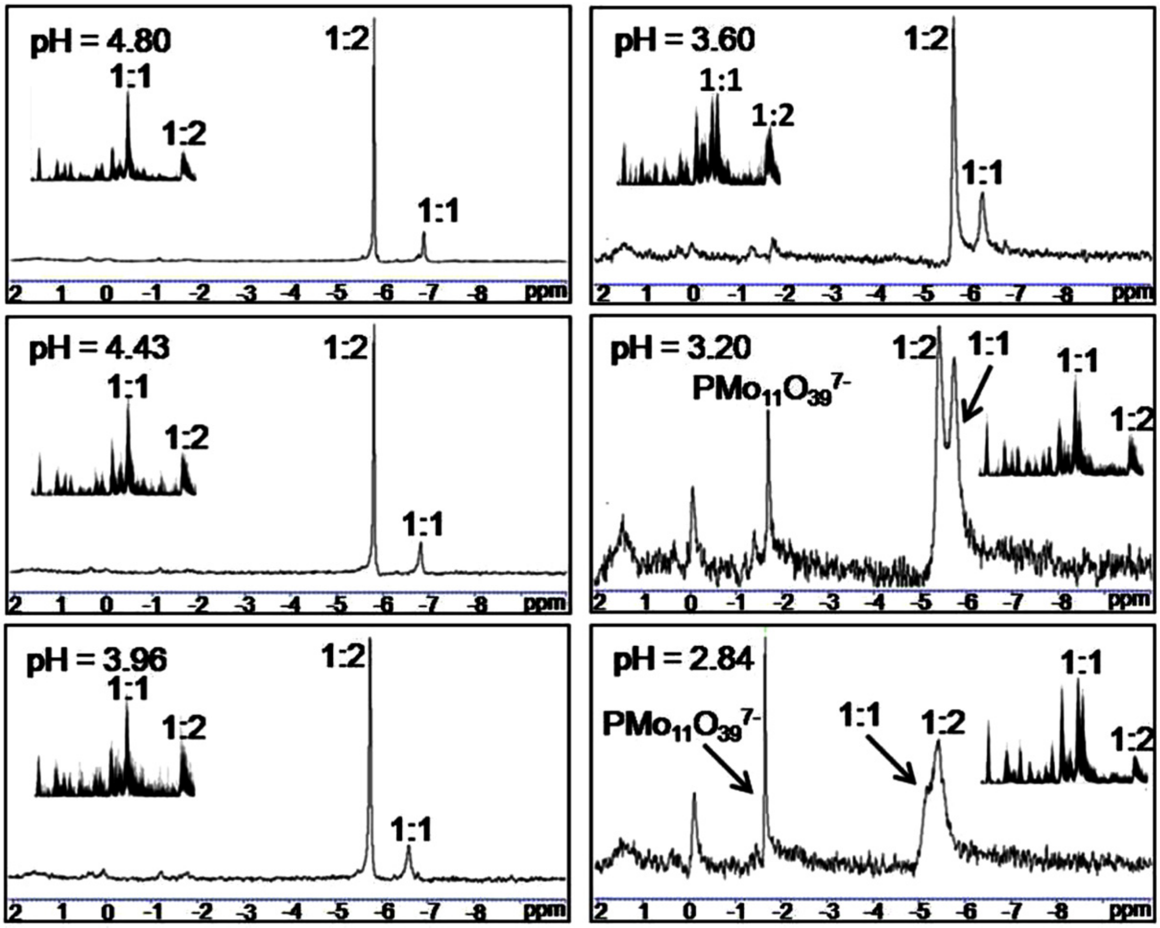

Fig. 8. ^{31}P NMR spectra of 11 mM Ce(III)POM at pH ranging from 4.80 (top left) to 2.84 (bottom right). Insets show ESI/MS spectra under the same conditions. Peak labels indicate Ce(III)PMo$_{11}$O$_{38}{}^{2-}$ (**1:1**) and H$_2$Ce(III)P$_2$Mo$_{22}$O$_{75}{}^{3-}$ (**1:2**) ions; the corresponding solution ion compositions are **1:1** H$_x$Ce(III)PMo$_{11}$O$_{39}{}^{(4-x)-}$ and **1:2** Ce(III)P$_2$Mo$_{22}$O$_{78}{}^{11-}$.

^{31}P NMR assignments are supported by ^{31}P NMR and ESI analyses of an 11 mM Ce(III)POM solution to which was added one equivalent of Ce^{3+} as Ce(NO$_3$)$_3$·6H$_2$O, which should drive the solution equilibrium towards the **1:1** complex. The result is the disappearance of the peaks attributed to the **1:2** complex in both ^{31}P NMR and ESI spectra (Fig. 7). In the solution with excess Ce^{3+}, the **1:1** complex is the only significant species observed in ESI/MS and, when compared to the ^{31}P NMR spectra, is assigned a chemical shift of −6.9 ppm in the 11 mM, pH 4.3 solution. The results of this experiment demonstrate that the species in the ESI mass spectra are directly representative of species in the precursor solution: when the **1:2** complex is absent in the solution, it is not seen by ESI/MS.

3.5.2. Varying pH; constant concentration

Dilution of the 11 mM CePOM solution is accompanied by a decrease in pH. Accordingly, spectral analyses of Ce(III)POM at a constant concentration were performed via ^{31}P NMR and ESI/MS while adjusting the pH from 4.8 to 2.8 in ~0.4 pH increments. The most notable effect across this pH range is a change in the ^{31}P NMR chemical shift of the **1:1** complex (Fig. 8) The change in this chemical shift is attributed to a change in the extent of solution protonation and, as a result, a change in the net charge of the complex [15]. In contrast to the **1:1** H$_x$Ce(III)PMo$_{11}$O$_{39}{}^{(4-x)-}$ complex, the change in the chemical shift for the **1:2** [Ce(III)(PMo$_{11}$O$_{39}$)$_2$]$^{11-}$ complex is minor across the studied pH range, indicating little if any protonation of the **1:2** complex with decreasing pH, as reflected by the un-protonated formulation. The chemical shift of the peak identified as the **1:1** complex – initially −6.9 ppm at pH 4.80 – eventually overtakes that for the **1:2** complex, appearing at −5.2 ppm at pH 2.84, further supporting its identification. The **1:1** complex should be more receptive towards protonation compared to the **1:2** complex. In the **1:1** complex, half of the cerium coordination environment is accessible to hydration and hydrolysis whereas in the **1:2** complex, all cerium coordination sites are shielded by the two POM ligands (Fig. 1). No significant pH effect is noted in the ESI/MS spectra, aside from an increase in the Ce(III)PMo$_{10}$O$_{35}{}^{2-}$ peak intensity (see Fig. 8, pH = 2.84; this enhanced peak is the intense peak appearing at lower *m*/*z* than the **1:1** peak). No discrete ^{31}P NMR signal is observed that can be assigned to the solution equivalent of this Ce(III)PMo$_{10}$O$_{35}{}^{2-}$ ion. Also present in the ^{31}P NMR spectra for pH 3.20 and 2.84 are peaks assigned to PMo$_{11}$O$_{39}{}^{7-}$, which indicates partial solution degradation of the Ce(III) POMs under these acidic conditions; this is consistent with the appearance of an ESI/MS species which corresponds to MoO$_3$-elimination from Ce(III)PMo$_{11}$O$_{38}{}^{2-}$.

3.5.3. Varying concentration; constant pH

To further deconvolute the interdependency of the solution and ESI/MS behavior on pH and concentration, spectra were taken for 11 mM, 5.6 mM, 1.1 mM, 0.56 mM, and 0.11 mM solutions of Ce(III)POM, all at a constant pH of 4.3 (Fig. 9). At 11 mM Ce(III)POM, both H$_2$Ce(III)P$_2$Mo$_{22}$O$_{75}{}^{3-}$ (**1:2**) and Ce(III)PMo$_{11}$O$_{38}{}^{2-}$ (**1:1**) are clearly present in ESI/MS and ^{31}P NMR spectra—it should be reiterated that the specified ESI/MS ion compositions differ from the solution compositions: in solution, the **1:2** complex is [Ce(III)(PMo$_{11}$O$_{39}$)$_2$]$^{11-}$ and the **1:1** complex is

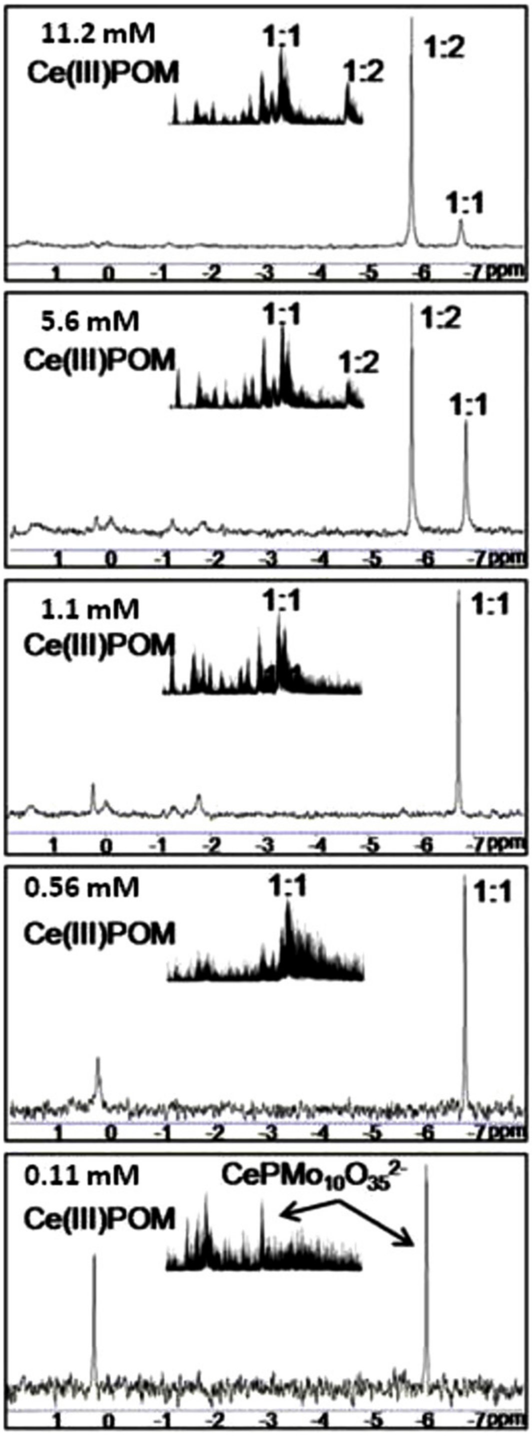

Fig. 9. ^{31}P NMR spectra of Ce(III)POM at pH = 4.3 ranging from 11 mM (top) to 0.11 mM (bottom). Insets show the corresponding ESI/MS spectra. Labels indicate **1:2** $H_2Ce(III)P_2Mo_{22}O_{75}^{3-}$, **1:1** $Ce(III)PMo_{11}O_{38}^{2-}$, and $Ce(III)PMo_{10}O_{35}^{2-}$; the **1:1** and **1:2** (and presumably $Ce(III)PMo_{10}O_{35}^{2-}$) solution compositions differ from the gas-phase compositions.

$H_xCe(III)P_2Mo_{11}O_{39}^{(4-x)-}$. The behavior of the 11 mM solution is similar to that observed for 5.6 mM. In contrast, the **1:2** complex is not found in either ESI/MS or NMR spectra in the 1.1 mM and 0.56 mM solutions. At a concentration of 0.11 mM, the **1:1** complex disappears and is evidently replaced by a phosphorous containing species with a chemical shift of −6.1 ppm. This change is also noted in the 0.11 mM ESI/MS spectrum, in which very little $Ce(III)PMo_{11}O_{38}^{2-}$ is observed and $Ce(III)PMo_{10}O_{35}^{2-}$ becomes pronounced. Another ^{31}P NMR signal at +0.3 ppm is seen growing in at 5.6 mM and is significant in 0.11 mM solutions. A concurrent increase in the relative intensity of $Ce(III)PMo_7O_{26}^{2-}$ in ESI/MS is also observed. This latter ion is the dominant species observed in ESI/MS analysis of 110 μM solutions and supports tentative assignment of chemical shifts of +0.3 ppm and −6.1 ppm to the solution precursors of the $Ce(III)PMo_7O_{26}^{2-}$ and $Ce(III)PMo_{10}O_{35}^{2-}$ ESI/MS ions, respectively, at pH 4.3. The identities and charges of the oxygen-saturated solution precursors of these ions remain unknown.

3.6. Solution and ESI speciation

Dominant ESI/MS Ce-containing species in concentrated solutions, produced from dissolving the precipitated 1:2 complex, are $H_2Ce(III)P_2Mo_{22}O_{75}^{3-}$ and $Ce(III)PMo_{11}O_{38}^{2-}$ (Fig. 2A). As discussed in Section 3.5, ^{31}P solution studies confirm that both complexes are present in solution, as $[Ce(III)(PMo_{11}O_{39})_2]^{11-}$ and $H_xCe(III)P_2Mo_{11}O_{39}^{(4-x)-}$, respectively, where x represents the variable extent of protonation of the **1:1** complex in solution. Notably, the relative abundances of the **1:2** and **1:1** complexes in the ESI spectra are not as in solution, as indicated by the ^{31}P NMR peak intensities: in the ESI spectra, the relative intensity of the **1:2** complex appears as much lower than its relative concentration in solution. This may partially result from variations in the trapping and detection sensitivity of the QIT/MS with increasing m/z. When the pH is not adjusted during dilution, a decrease in pH from 4.3 to 3.6 is observed upon dilution from 11 mM to 0.7 mM. ^{31}P NMR spectra also reveal the presence of free ligand, $H_xPMo_{11}O_{39}^{(7-x)-}$, in dilute Ce(III)POM solutions. Combined, these observations suggest an equilibrium shift in solution upon dilution from the **1:2** sandwich complex to a singly-bound **1:1** Ce-complex, along with hydrolysis of the Ce ion. Eq. (8a) gives such an idealized solution reaction (denoted as "in situ"); Eq. (8b) hypothesizes the subsequent ESI reaction to yield $Ce(III)PMo_{11}O_{38}^{2-}$ from $(OH)_xCe(III)PMo_{11}O_{39}^{(4+x)-}$ solution species. Based on the absence of $Ce(III)PMo_{11}O_{38}^{2-}$ in any of the CID spectra of $H_2Ce(III)P_2Mo_{22}O_{75}^{3-}$, it is concluded that the **1:1** complex is not produced through gas fragmentation of precursors during ion transport. However, the possibility of a **1:2** to **1:1** conversion during the spray processes of droplet desolvation and analyte charge reduction cannot be ruled out.

$$xH_2O_{(aq)} + Ce(III)(PMo_{11}O_{39})_{2\,(aq)}^{11-} \xrightarrow{\text{in situ}} PMo_{11}O_{39\,(aq)}^{7-} + xH^+_{(aq)} + (OH)_xCe(III)PMo_{11}O_{39\,(aq)}^{(4+x)-} \tag{8a}$$

$$(x+2)\,H^+_{(aq)} + (OH)_xCe(III)PMo_{11}O_{39\,(aq)}^{4+x}(x+1)\,H_2O_{(g)} + Ce(III)PMo_{11}O_{38\,(g)}^{2-} \tag{8b}$$

Formation of the new species, $Ce(III)PMo_{10}O_{35}^{2-}$, at low concentration might be attributed to several potential processes, including: (1) the ejection of a neutral plenary phosphomolybdate, $H_3PMo_{12}O_{40}$ (Eq. (9a)), during ESI, (2) successive fragmentation (generically denoted as "Frag") of solution parent species through the ESI and ion transport processes (e.g., Eqs. (9b) and (9c)), or (3) a stable solution species formed most favorably at lower concentrations. However, as this new species is noted from solutions which do not contain the **1:2** complex, and its presence and intensity do not correlate with the ESI/MS intensity of the **1:1** complex (Fig. 2), Eqs. (9a)–(9c), as well as other gas-phase processes, can be excluded as feasible explanations. It is therefore concluded that the precursor of $Ce(III)PMo_{10}O_{35}{}^{-}{}_{(g)}$ is a new stable solution species formed

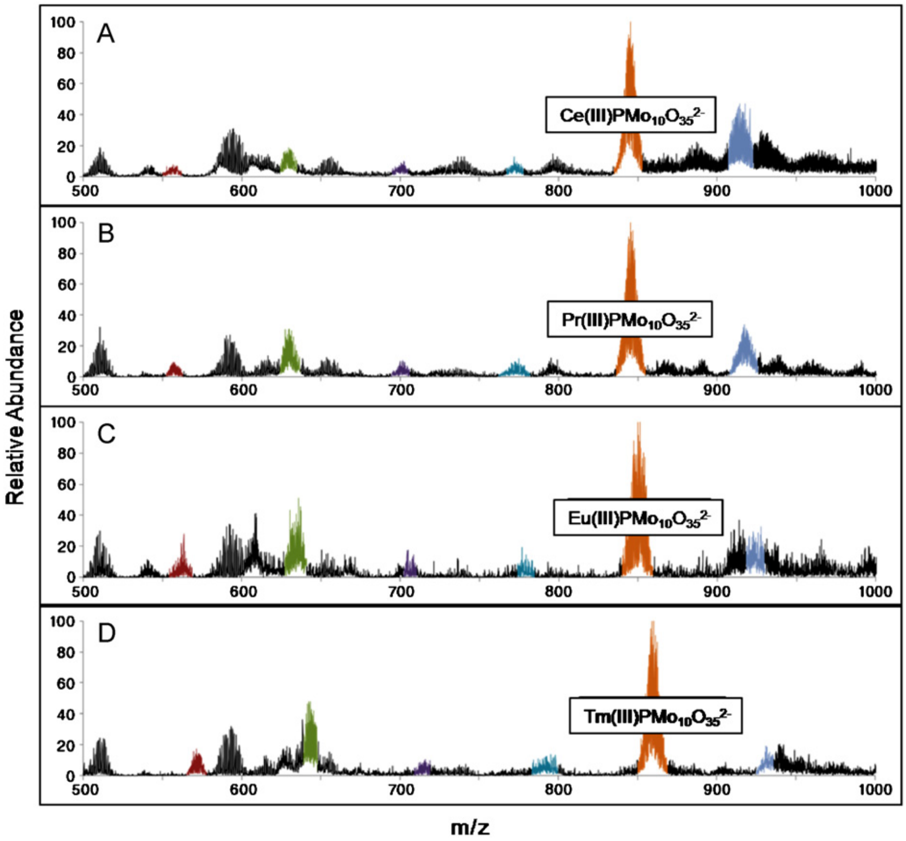

Fig. 10. Spectra taken from aqueous solutions of (A) 0.7 mM Ce(III)POM, (B) 1.2 mM Pr(III)POM, (C) 1.3 mM Eu(III)POM, and (D) 1.2 mM Tm(III)POM. Highlighted Ln-phosphomolybdate ions are Ln(III)$PMo_6O_{23}{}^{2-}$ (red), Ce(III)$PMo_7O_{26}{}^{2-}$ (green), Ce(III)$PMo_8O_{29}{}^{2-}$ (purple), Ce(III)$PMo_9O_{32}{}^{2-}$ (teal), Ce(III)$PMo_{10}O_{35}{}^{2-}$ (orange), and Ce(III)$PMo_{11}O_{38}{}^{2-}$ (grey). Non-highlighted species do not contain a lanthanide. (For interpretation of the references to colour in this figure legend, the reader is referred to the web version of the article.)

at low concentrations.

$$H_3Ce(III)P_2Mo_{22}O^{2-}_{75(aq)} \xrightarrow{ESI} H_3PMo_{12}O_{40(g)} + Ce(III)PMo_{10}O^{2-}_{35(g)} \tag{9a}$$

$$\begin{aligned} HCe(III)P_2Mo_{22}O^{4-}_{75(g)} &\xrightarrow{Frag} HMo_4O^{-}_{13(g)} + Ce(III)P_2Mo_{18}O^{3-}_{62(g)} \\ &\xrightarrow{Frag} PMo_5O^{-}_{18(g)} + Ce(III)PMo_{13}O^{2-}_{44(g)} \\ &\xrightarrow{Frag} Mo_3O_{9(g)} + Ce(III)PMo_{10}O^{2-}_{35(g)} \end{aligned} \tag{9b}$$

$$Ce(III)PMo_{11}O^{2-}_{38(g)} \xrightarrow{Frag} MoO_{3(g)} + Ce(III)PMo_{10}O^{2-}_{35(g)} \tag{9c}$$

3.7. Variations in speciation across the LnPOM series

ESI/MS spectra were acquired for 0.7 mM–1.3 mM Ln(III)POMP$Mo_{10}O_{35}{}^{2-}$ solutions for Ln = Ce, Pr, Eu and Tm (Fig. 10) The appearance of Ln(III)$PMo_{10}O_{35}{}^{2-}$ as the dominant ion occurs across the Ln series. While the main features remain invariant, Ln(III)$PMo_{11}O_{38}{}^{2-}$ is most prominent for Ce and clearly decreases in relative abundance across the series; the opposite is true for the smaller Ln-phosphomolybdate species, Ln$PMo_6O_{23}{}^{2-}$ and Ln$PMo_7O_{26}{}^{2-}$, which increase in relative abundance across the series. A detailed understanding of these variations in ESI/MS spectra is beyond the scope of this work.

3.8. Relationship between gas- and condensed-phase complexes

A key issue raised by these results is whether or not connections can be made between observed gas-phase species and stable lanthanide-polyoxometalate species which exist in condensed phases. In contrast to Ce$PMo_{11}O_{38}{}^{2-}$, the bare or protonated Ce(III)$PMo_{10}O_{35}{}^{2-}$ ion, formed through CID (Eq. (4a)) and present as presumably an oxo-saturated ion in solution (see Section 3.6), is a new moiety to phosphomolybdate chemistry; isolation of Ce(III)$PMo_{10}O_{35}{}^{2-}$ presents a rare example of large ion complexes resulting independently from both solution and gas-phase dissociation.

The novel cerium heteropolyoxotungstate crystal, $H_7K_{10}[Ce_2(IV)(PW_{10}O_{38})(PW_{11}O_{39})_2]\cdot 28H_2O$ [21], forms upon slow evaporation of dilute solutions of ceric ammonium nitrate and phosphotungstic acid *after* precipitation and removal of the primary product, $K_{10}[Ce(IV)(PW_{11}O_{39})_2]\cdot 8H_2O$. The conditions for which Ce(III)$PMo_{10}O_{35}{}^{2-}$ was observed in solution – i.e., low concentrations (Fig. 2) – match those under which this novel Ce(IV) complex was synthesized [21]. The observation of a Ce(III) solution poloxomolybdate under conditions similar to those for synthesis of a Ce(IV) polyoxotungstate may indicate analogous growth mechanisms, and possibly also a structural relationship. The discrete V-shaped dimeric complex $H_7K_{10}[Ce_2(IV)(PW_{10}O_{38})(PW_{11}O_{39})_2]\cdot 28H_2O$ is constructed from mono- and bi-vacant lacunary Keggin-type anions bridged by Ce(IV) cations, i.e., $[(PW_{11}O_{39})–Ce–(PW_{10}O_{38})–Ce–(PW_{11}O_{39})]^{17-}$. The formula and growth mechanisms suggest that the structure of

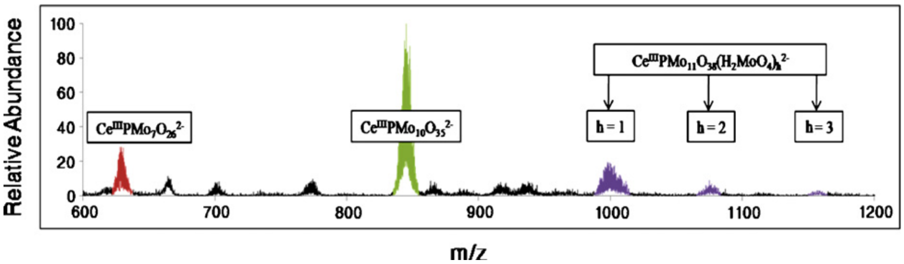

Fig. 11. Spectra of Ce(III)POM at 0.7 mM taken ∼48 h after dilution. Highlighted species are Ce(III)$PMo_7O_{26}{}^{2-}$, Ce(III)$PMo_{10}O_{35}{}^{2-}$, and Ce(III)$PMo_{11}O_{38}(H_2MoO_4)_h{}^{2-}$ (h = 1, 2, 3).

gaseous Ce(III)$PMo_{10}O_{35}{}^{2-}$ may be related to the Ce–($PW_{10}O_{38}$) moiety in the dimeric solid complex.

The stoichiometry of the CID product HCe(III)$P_2Mo_{18}O_{62}{}^{2-}$ from H_2Ce(III)$P_2Mo_{22}O_{75}{}^{3-}$ (Eq. (2a)) provokes the hypotheses that Ce(III) in this product may be sandwiched between two trivacant lacunary Keggin anions ($PMo_9O_{31}{}^{3-}$), or complexed by a protonated Dawson-Wells type phosphomolybdate ($P_2Mo_{18}O_{62}{}^{6-}$). Both of these anion structures are known in phosphotungstate chemistry [19,21–24]. Condensed phase results do not support the first hypothetical structure for the cerium complexes as crystal structures suggest that the vacancy in the trivacant lacunary Keggin ion is too large to complex a Ln ion; however it does effectively coordinate the actinyl cation ($AnO_2{}^{2+}$) through equatorial binding sites due to the steric hindrance imposed by these species [25–27]. Also, only plenary Keggin ions have been shown to complex tetravalent transition metals, i.e., Zr and Hf [18]; to our knowledge, there are no analogous complexes with plenary Dawson-Wells ions. Instead, structural Ln-phosphotungstate results suggest that Ce(III) is complexed by a $P_2Mo_{17}O_{58}{}^{4-}$ lacunary Dawson-Wells ion and a molybdate anion ($MoO_4{}^{2-}$) [28]. This postulated structure is based on the observation that the lacunary Dawson-Wells polyoxoanion $P_2W_{17}O_{61}{}^{10-}$ binds Ln(III) ions much more effectively than does the non-lacunary $P_2W_{18}O_{62}{}^{6-}$ [28]. Although reasonable structures such as this can be postulated based on condensed phase chemistry, computational studies are needed to support such hypothetical structures of large gas-phase complexes.

3.9. Cluster degradation and reassembly in solution

ESI of the 0.7 mM CePOM solution allowed to age approximately 48 h exhibits new peaks assigned as Ce(III)$PMo_{11}O_{38}(H_2MoO_4)_h{}^{2-}$ (h = 1–3; Fig. 11). This observation suggests formation of H_2MoO_4 via solution degradation of clusters, and consequent assembly of new clusters by association with these degradation fragments. CID results for these new clusters are shown in Fig. 12. Ce(III)$PMo_{11}O_{38}H_2MoO_4{}^{2-}$ and Ce(III)$PMo_{11}O_{38}(H_2MoO_4)_3{}^{2-}$ fragment almost exclusively through loss of a single neutral H_2MoO_4 (Fig. 12A and C). In contrast, Ce(III)$PMo_{11}O_{38}(H_2MoO_4)_2{}^{2-}$ distinctively degrades through multiple pathways (Fig. 12B), listed below (Eqs. (10a)–(10d)) in order of decreasing relative abundances, to form H_4Ce(III)$Mo_{10}O_{34}{}^{-}$, Ce(III)$PMo_{12}O_{41}{}^{2-}$, H_2Ce(III)$PMo_{12}O_{42}{}^{2-}$, and H_4Ce(III)$Mo_9O_{31}{}^{-}$. The distinctive behavior of Ce(III)$PMo_{11}O_{38}(H_2MoO_4)_2{}^{2-}$ is indicative of structural rearrangement in the parent species or during the CID process; in contrast the other two species exhibit CID behavior characteristic of elimination of H_2MoO_4 adducts.

$$\mathrm{Ce(III)PMo_{11}O_{38}(H_2MoO_4)^{2-}_{2\,(g)}} \xrightarrow{\mathrm{CID}} \mathrm{PMo_3O_{12}{}^{-}{}_{(g)}} + \mathrm{H_4Ce(III)Mo_{10}O_{34}{}^{-}{}_{(g)}} \tag{10a}$$

$$\mathrm{Ce(III)PMo_{11}O_{38}(H_2MoO_4)^{2-}_{2\,(g)}} \xrightarrow{\mathrm{CID}} H_2MoO_{4\,(g)} + H_2O_{(g)} + \mathrm{Ce(III)PMo_{12}O^{2-}_{41\,(g)}} \tag{10b}$$

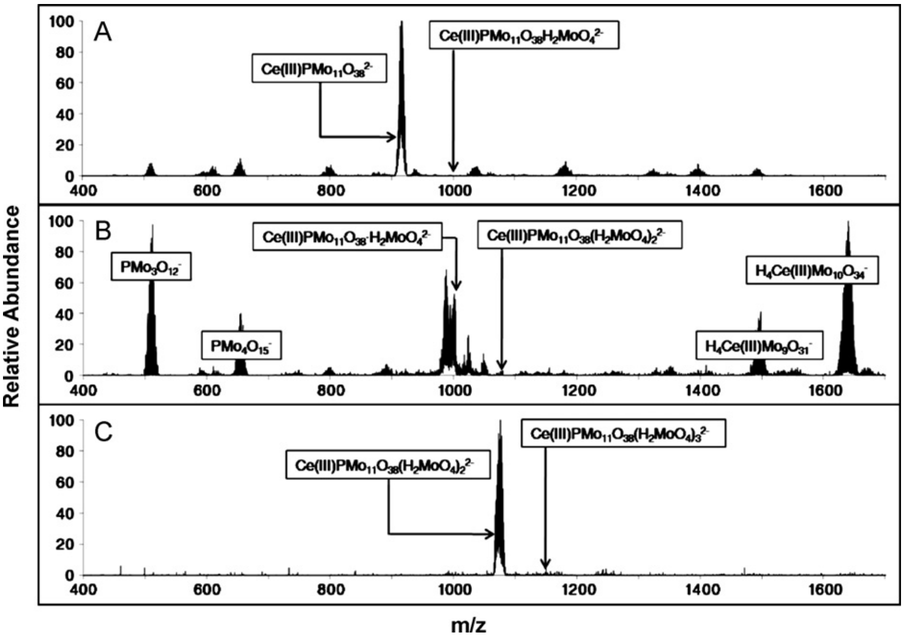

Fig. 12. CID of (A) Ce(III)$PMo_{11}O_{38}(H_2MoO_4)^{2-}$, (B) Ce(III)$PMo_{11}O_{38}(H_2MoO_4)_2{}^{2-}$, and (C) Ce(III)$PMo_{11}O_{38}(H_2MoO_4)_3{}^{2-}$ from 0.7 mM Ce(III)POM solution illustrating the distinctive behavior of Ce(III)$PMo_{11}O_{38}(H_2MoO_4)_2{}^{2-}$. Not labeled in (B) is the CID product Ce(III)$PMo_{12}O_{41}{}^{2-}$ at m/z 9 below Ce(III)$PMo_{11}O_{38}H_2MoO_4{}^{2-}$.

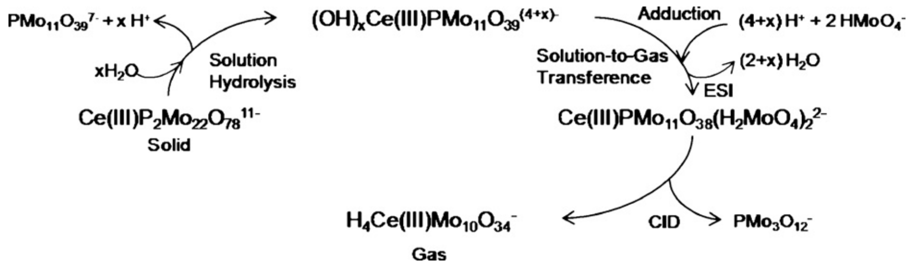

Scheme 1. Proposed solid/solution/gas reaction pathway for production of $H_4CePMo_{10}O_{34}^-$ from $[Ce(III)(PMo_{11}O_{39})_2]^{11-}$ (i.e., $Ce(III)P_2Mo_{22}O_{78}{}^{11-}$ in solid and solution).

$$Ce(III)PMo_{11}O_{38}(H_2MoO_4)^{2-}_{2(g)} \xrightarrow{CID} H_2MoO_{4(g)} + H_2Ce(III)PMo_{12}O^{2-}_{42(g)} \qquad (10c)$$

$$Ce(III)PMo_{11}O_{38}(H_2MoO_4)^{2-}_{2(g)} \xrightarrow{CID} PMo_4O_{15^-(g)} + H_4Ce(III)Mo_9O_{31^-(g)} \qquad (10d)$$

The empirical formula of $H_4Ce(III)Mo_{10}O_{34}{}^-$, formed from degradation of $Ce(III)PMo_{11}O_{38}(H_2MoO_4)_2{}^{2-}$, differs by two waters from the first reported Ln-polyoxometalate complex, $[Ln(III)W_{10}O_{36}]^{9-}$, the structure of which consists of the 8-coordinate Ln(III) cation sandwiched between two $[W_5O_{18}]^{6-}$ anions [29]. The proposed route to the formation of $H_4Ce(III)Mo_{10}O_{34}{}^-$ is a case where speciation can be followed from solid to gas, incorporating the chemical process of dissolution, equilibrium shift and hydrolysis, cluster formation, transference to gas, and gas-phase ion degradation, as represented in Scheme 1.

4. Conclusions

ESI/MS has been utilized to successfully transfer large Ln-phosphomolybdate sandwich-structures from aqueous solutions to the gas phase. The ion $H_2Ce(III)P_2Mo_{22}O_{75}{}^{3-}$ is observed and is evidently produced from protonation of the $[Ce(III)(PMo_{11}O_{39})_2]^{11-}$ parent solution ion, and water loss during ESI. CID was used to identify large isotopically complex ions by systematic fragmentation into smaller ions. Connections are made between gaseous ions (e.g., $Ce(III)PMo_{10}O_{35}{}^{2-}$, $HCe(III)P_2Mo_{18}O_{62}{}^{2-}$, $Ce(III)PMo_{11}O_{38}(H_2MoO_4)_2{}^{2-}$, and $H_4Ce(III)Mo_{10}O_{34}{}^-$) and known condensed-phase species. ^{31}P NMR was used to relate solution speciation to ions observed by ESI/MS. Solution speciation of the parent **1:2** complex shows dynamic behavior dependent on solution concentration, with both solution degradation and fragment aggregation processes becoming significant at low concentrations. The speciation under ESI behavior evolves with decreasing concentration from $H_2Ce(III)P_2Mo_{22}O_{75}{}^{3-}$ to $Ce(III)PMo_{11}O_{38}{}^{2-}$ to $Ce(III)PMo_{10}O_{35}{}^{2-}$ as dominant species. These results are attributed to an equilibrium shift between the **1:2** and **1:1** complex; the appearance of the molybdenum-deficient $CePMo_{10}O_{35}{}^{2-}$ ion was not anticipated and remains enigmatic.

At low concentrations, new cluster species form through the successive net addition of neutral H_2MoO_4 molecules to $Ce(III)PMo_{11}O_{38}{}^{2-}$; this is a new development in cluster degradation/aggregation chemistry. Additionally, CID indicated that structural rearrangement occurs in the specific case of $Ce(III)PMo_{11}O_{38}(H_2MoO_4)_2{}^{2-}$. Based on the assigned compositions, it was concluded that the parent Ce(III) solution oxidation state was retained for the studied ESI and CID processes. This latter conclusion is not necessarily surprising, but an important aspect of this work was the substitution of $^7Li^+$ for $^1H^+$ in solution and gas-phase ions, which enabled obtaining accurate counter-ion counts, and thus the cerium oxidation state. We have developed a method for accurately determining the oxidation state of the complexed metal ion; this will be useful in the future investigations of redox-active f-element complexes containing Ce(IV) and Pu(III/IV).

Acknowledgments

The authors thank Dr. Wayne Lukens and Dr. Rebecca Abergel for suggestions and assistance, and Dr. Philip Rutkowski for critical comments on the manuscript. This research was supported by the Director, Office of Science, Office of Basic Energy Sciences, Division of Chemical Sciences, Geosciences, and Biosciences of the U.S. Department of Energy at LBNL under Contract No. DE-AC02-05CH11231.

References

[1] A few recent pertinent POM reviews: D.L. Long, R. Tsunashima, L. Cronin, Angew. Chem. Int. Ed. 49 (2010) 1736;
P. Kogerler, B. Tsukerblat, A. Muller, Dalton Trans. 21 (2010);
K. Binnemans, Chem. Rev. 109 (2009) 4283;
H.N. Miras, E.F. Wilson, L. Cronin, Chem. Commun. (2009) 1297.

[2] J. Le Quan Tuoi, E. Muller, Rapid. Commun. Mass Spectrom. 8 (1994) 692.

[3] T.-C. Lau, J. Wang, R. Guevremont, K.W.M. Siu, Chem. Commun. (1995) 977.

[4] M.J. Deery, O.W. Howarth, K.R. Jennings, Dalton Trans. (1997) 4783.

[5] D.K. Walanda, R.C. Burns, G.A. Lawrance, E.I. von Nagy-Felsobuki, Dalton Trans. (1999) 311.

[6] D.K. Walanda, R.C. Burns, G.A. Lawrance, E.I. von Felsobuki, Inorg. Chem. Commun. (1999) 487.

[7] D.K. Walanda, R.C. Burns, G.A. Lawrance, E.I. von Felsobuki, J. Cluster Sci. 11 (2000) 5.

[8] C.E. Easterley, D.M. Hercules, M. Houallo, Appl. Spectrosc. 55 (2001) 1665.

[9] C.E. Easterley, D.M. Hercules, M. Houallo, Appl. Spectrosc. 55 (2001) 1671.

[10] M. Bonchio, O. Bortolini, V. Conte, A. Sartorel, Eur. J. Inorg. Chem. 4 (2003) 699.

[11] M.T. Ma, T. Waters, K. Beyer, R. Palamarczuk, P.J.S. Richardt, R.A.J. O'Hair, A.G. Wedd, Inorg. Chem. 48 (2009) 598.

[12] V.B. Di Marco, G.G. Bombi, Mass Spectrom. Rev. 25 (2006) 347.

[13] G.J. Van Berkel, V. Kertesz, Anal. Chem. 79 (2007) 5510.

[14] A.J. Gaunt, I. May, M.J. Sarsfield, D. Collison, M. Helliwell, I.S. Denniss, Dalton Trans. (2003) 2767.

[15] R. Copping, A.J. Gaunt, I. May, M.J. Sarsfield, D. Collison, M. Helliwell, I.S. Denniss, D.C. Apperly, Dalton Trans. (2005) 1256.

[16] M. Sadakane, M.H. Dickman, M.T. Pope, Angew. Chem. Int. 39 (2000) 16.

[17] A.J. Gaunt, I. May, D. Collison, O.D. Fox, Inorg. Chem. 42 (2003) 5049.

[18] R. Copping, L. Johansson, A.J. Gaunt, D. Drennan, D. Collison, M. Helliwell, R.J. Pirttijarvi, C.J. Jones, A. Huguet, D.C. Apperley, N. Kaltsoyannis, I. May, Inorg. Chem. 47 (2008) 5787.

[19] C. Boglio, G. Lenoble, C. Duhayon, B. Hasenknopf, R. Thouvenot, C. Zhang, R.C. Howell, B.P. Burton-Pye, L.C. Francesconi, E. Lacôte, S.C. Thorimbert, J.-C. Tabet, Inorg. Chem. 45 (2006) 1389.

[20] T.H. Bray, R. Copping, D.K. Shuh, J.K. Gibson, in: J.K. Gibson, S.K. McCall, E.D. Bauer, L. Soderholm, T. Fanghaenel, R. Devanathan, C. Misra, C. Trautmann, B.D. Wirth (Eds.), Basic Actinide Science and Materials for Nuclear Applications, Materials Research Society, Warrendale, PA, 2010.

[21] F.L. Sousa, F.A. Almeida Paz, A.M.V. Cavaleiro, J. Klinowski, H.I.S. Nogueira, Chem. Commun. (2004) 2656.

[22] R.C. Howell, F.G. Perez, S. Jain, W.De W. Horrocks Jr., A.L. Rheingold, L.C. Francesconi, Angew. Chem. Int. Ed. 40 (2001) 4031.

[23] A.J. Gaunt, I. May, D. Collison, M. Helliwell, Acta Cryst. (2003), C59, i65.

[24] C.R. Mayer, C. Roch-Marchal, H. Lavanant, R. Thouvenot, N. Sellier, J.-C. Blais, F. Sécheresse, Chem. Eur. J. 10 (2004) 5517.
[25] R. Copping, C. Talbot-Eeckelaers, D. Collison, M. Helliwell, A.J. Gaunt, I. May, S.D. Reilly, B.L. Scott, R.D. McDonald, O.A. Valenzula, C.J. Jones, M.J. Sarsfield, Dalton Trans. 29 (2009) 5609.
[26] R. Copping, A.J. Gaunt, C.A. Sharrad, D. Collison, M. Helliwell, D.O. Fox, C.J. Jones, Chem. Commun. 36 (2006) 3788.
[27] A.J. Gaunt, I. May, R. Copping, A.I. Bhatt, D. Collsion, D.O. Fox, K.T. Holman, M.T. Pope, Dalton Trans. 15 (2003) 3009.
[28] Q.-H. Luo, R.C. Howell, M. Dankova, J. Bartis, C.W. Williams, W.DeW. Horrocks Jr., V.G. Young Jr., A.L. Rheingold, L.C. Franscesconi, M.R. Antonio, Inorg. Chem. 40 (2001) 1894.
[29] P.D. Peacock, T.J.R. Weakley, J. Chem. Soc. A: Inorg. Phys. Theor. (1971) 1836.